doi:10.1006/jmbi.2001.4978 available online at http://www.idealibrary.com on IDEAL® J. Mol. Biol. (2001) 312, 525–540

JMB

Structural and Functional Linkages Between Subunit Interfaces in Mammalian Pyruvate Kinase

John O. Wooll, Robert H. E. Friesen, Mark A. White Stanley J. Watowich, Robert O. Fox, J. Ching Lee* and Edmund W. Czerwinski*

Department of Human Biological Chemistry and Genetics and the Sealy Center for Structural Biology, The University of Texas Medical Branch, Galveston, TX 77555-0647, USA

**Corresponding authors*

Mammalian pyruvate kinase (PK) is a four-domain enzyme that is active as a homo-tetramer. Tissue-specific isozymes of PK exhibit distinct levels of allosteric regulation. PK expressed in muscle tissue (M_1-PK) shows hyperbolic steady-state kinetics, whereas PK expressed in kidney tissue (M_2-PK) displays sigmoidal kinetics. Rabbit M_1 and M_2-PK are isozymes whose sequences differ in only 22 out of 530 residues per subunit, and these changes are localized in an inter-subunit interface. Previous studies have shown that a single amino acid mutation to M_1-PK at either the Y (S402P) or Z (T340 M) subunit interface can confer a level of allosteric regulation that is intermediate to M_1-PK and M_2-PK. In an effort to elucidate the roles of the inter-subunit interaction in signal transmission and the functional/structural connectivity between these interfaces, the S402P mutant of M_1-PK was crystallized and its structure resolved to 2.8 Å. Although the overall S402P M_1-PK structure is nearly identical with the wild-type structure within experimental error, significant differences in the conformation of the backbone are found at the site of mutation along the Y interface. In addition, there is a significant change along the Z interface, namely, a loss of an inter-subunit salt-bridge between Asp177 of domain B and Arg341 of domain A of the opposing subunit. Concurrent with the loss of the salt-bridge is an increase in the degree of rotational flexibility of domain B that constitutes the active site. Comparison of previous PK structures shows a correlation between an increase in this domain movement with the loss of the Asp177: Arg341 salt-bridge. These results identify the structural linkages between the Y and Z interfaces in regulating the interconversion of conformational states of rabbit M_1-PK.

© 2001 Academic Press

Keywords: pyruvate kinase; allosterism; subunit communication; structure; X-ray crystallography

Introduction

Maintenance of the flux of energy and material within a cell is essential for homeostasis and function. Fundamental energy production in the cell is found within the glycolytic pathway, the regulation of which is primarily associated with two allosteric enzymes. Phosphofructokinase coordinates the process down the pathway of glycolysis. Passage out of glycolysis is modulated by pyruvate kinase (PK; E.C. 2.7.1.40) that catalyzes the transfer of the phosphate from P-enolpyruvate (PEP) to ADP.[1–7]

$$\mathrm{PEP} + \mathrm{ADP} \overset{\mathrm{PK}}{\Longleftrightarrow} \mathrm{ATP} + \mathrm{Pyruvate}$$

Mammalian PK is a homo-tetramer, and each subunit consists of four domains (Figure 1(a)). The catalytic activity of PK is proposed to be activated by the "clamping down" or "closing" of the B

Present; address: R. H. E. Friesen, Biomade Technology Foundation, Nijenborgh 4, 9747 AG Groningen, The Netherlands.

Abbreviations used: PK, pyruvate kinase; PEP, P-enolpyruvate; M_1-PK, muscle PK isozyme; M_2-PK, kidney PK isozyme; rRMPK, recombinant rabbit muscle PK; FBP, fructose 1,6-bisphosphate; YPK, yeast PK.

E-mail addresses of the corresponding authors: edcz@hbcg.utmb.edu; jclee@utmb.edu

0022-2836/01/030525–16 $35.00/0 © 2001 Academic Press

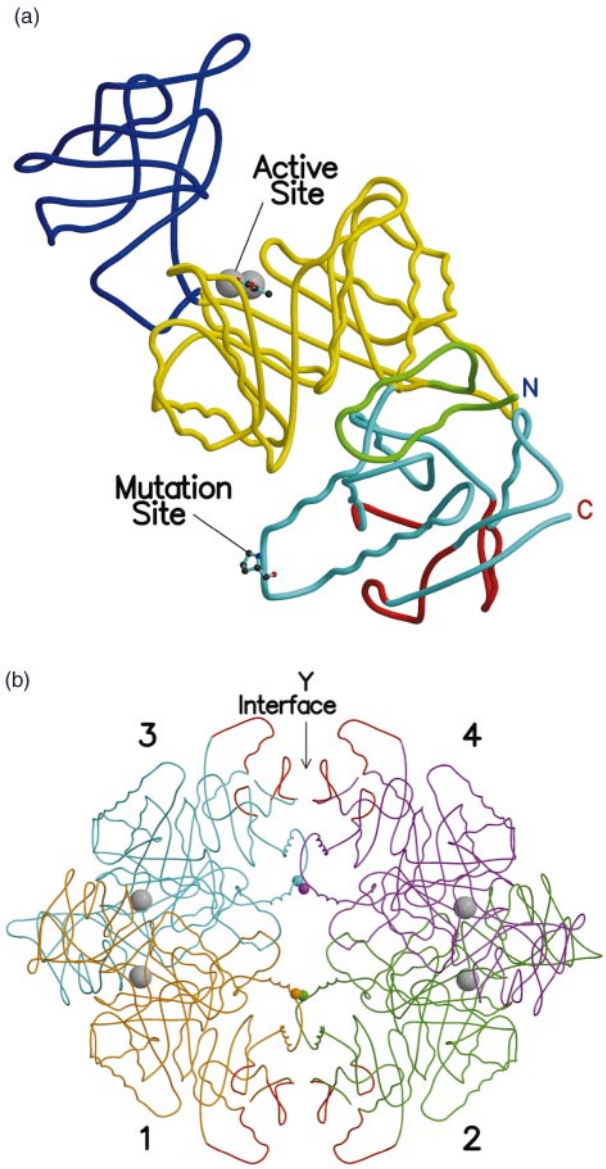

Figure 1. (a) View of the S402P monomer structure showing overall view of the monomer with the domains colored, A (yellow), B (blue), C (cyan) and N (green). The putative FBP binding region of the S402P structure is shown in red. (b) View of the S402P structure perpendicular to the Y interface separating monomers 1 and 3 from monomers 2 and 4.[5] The Z interface separates monomers 1 and 2 from 3 and 4. The Z interface is convoluted as monomers 1 and 2 wrap around monomers 3 and 4, respectively, like clasping hands. Large gray spheres represent the locations of the active site in each monomer. The smaller colored spheres represent the sites of mutation, which are ~40 Å from their respective active site. The putative FBP binding region of the S402P structure is shown in red.

domain (residues 116-218) onto the A domain (residues 43-115 and 219-387), thus dehydrating the interceding cleft that makes up the active site.[8,9] The role of the other two domains, C (residues 388-530) and N (residues 1-42) are less well characterized. But these domains are situated at sites of inter-subunit contact, and therefore, may play essential roles in assembly and intermolecular communication (Figure 1(b)).

Central to this investigation are the differentially regulated PK isozymes muscle PK (M_1-PK) and kidney PK (M_2-PK) that are products of alternative splicing of a single gene. In rabbit, M_1 and M_2-PK are isozymes with 530 amino acid residues in each subunit. They differ in 22 residues localized in the C domain along the Y inter-subunit interface.[10–12] M_1-PK is the major isozyme of skeletal muscle. It is a stable homo-tetramer that shows hyperbolic steady-state kinetics, and is relatively insensitive to effectors, requiring millimolar concentrations to elicit an effect. M_2-PK expression is more ubiquitous, and is the major isozyme in the kidney and leukocytes. It shows sigmodal steady-state kinetics. It is activated by fructose 1,6-bisphosphate (FBP) and is inhibited by phenylalanine at micromolar concentrations. Furthermore, M_2-PK has been shown to undergo reversible dimer-tetramer association, probably allowing an added level of regulatory control.[12,13]

Previous studies[3,6] on these PK isozymes suggest that the regulatory behavior can be described by a two-state model.[14] This model proposes an active (R) and an inactive (T) form of a macromolecule with differential affinities for ligands. The binding of the inhibitor phenylalanine to the M_1-PK has been shown to produce a global structural change.[7] The phenylalanine-bound enzyme exhibits a reduced affinity for the substrate, PEP. These observations are consistent with an $R \rightarrow T$ transition induced by phenylalanine binding.[2,3,15] In the M_2 system, transition between the R and T form due to effector interaction is more pronounced. Not only is a similar behavior seen with the inhibitor phenylalanine at lower concentrations, it has been shown that PEP enhances subunit interactions while ADP has the opposite effect.[12] It is evident that various metabolites bind to PK and elicit different signals transmitted through subunit interfaces. Understanding the distribution of M_1-PK and M_2-PK between the active and inactive state must ultimately link the different molecular behaviors of M_1-PK and M_2-PK to the differences in sequence encoded by these alternatively spliced exons.

A strategy was developed to elucidate the molecular mechanism in conferring allostery in PK based on the sequence differences and enzyme regulatory patterns of PK isozymes.[10] In an effort to elucidate the role(s) of inter-subunit interactions in signal transmission and the functional/structural connectivity between these interfaces, mutations at these interfaces were generated in the context of the M_1-PK sequence based on sequence differences between the M_1 and M_2-PK isozymes. Thus, the inter-subunit interaction between the C domains of adjacent subunits along the Y interface was modified by a S402P mutation.[10–12,16] Furthermore, the

choice of a S402P mutation is based on the result of a computational study which shows a significant structural perturbation at the point of mutation. The perturbation leads to a formation of an alternative inter-subunit salt-bridge involving the conserved Lys421.[10] Converting Ser402 to Pro changes neither the secondary, nor the tetrameric structure, as measured by circular dichroism and sedimentation velocity, respectively. However, the S402P mutant exhibits steady-state kinetic behavior that indicates that the mutant is more responsive to regulation by effectors. In another study to probe the Z interface, the inter-subunit interaction between the A and B domain of adjacent subunits was perturbed with a T340M mutation.[11] Although the mutations are at different interfaces, qualitatively the T340M and S402P M_1-PK mutants elicit similar kinetic effects, namely, greater sensitivity to inhibition by phenylalanine and decreased responsiveness to activation by FBP. More significantly, the T340 M mutation enhances the affinity of subunit-subunit interaction along the Y interface in M_2-PK.[12,13,16] These results indicate that the two different subunit interfaces are functionally connected, and that the pathways of signal transmission traverse both interfaces. A detailed understanding of the molecular mechanism of signal transmission and allostery in PK requires structural information of PK mutants at these subunit interfaces. Thus, the crystal structures of the recombinant rabbit muscle M_1-PK (rRMPK) wild-type enzyme and the S402P M_1-PK mutant were determined. A comparison between these structures is reported.

Results

Quality of the structures

The *P*1 unit cell of the S402P M_1-PK and rRMPK crystals each contain two PK tetramers arranged along a pseudo 2-fold axis nearly co-incident with the crystallographic **a** axis. Although the orientation of the tetramers is similar in the two proteins, lattice contacts differ in the two crystals. Most notably, there are inter-monomeric contacts in the rRMPK crystal, which may account for the reorientation of residues 514 to 518 observed in the rRMPK crystal but not in the S402P M_1-PK or the 1PKN structure.[17] Comparison of the rRMPK and 1PKN structures, crystallized under similar conditions, confirms the high degree of structural similarity even at the sites of the sequence discrepancies (D233E, E234Q, and S400A).[11] The 8-fold, non-crystallographic symmetry refinement of the rRMPK structure, in which all monomers are identical, resulted in *R*-factor and R_{free} of 0.239 and 0.247, respectively. Although the 1PKN structure was solved to a slightly higher resolution than the rRMPK structure (2.9 Å *versus* 3.0 Å) the rmsd of the C^{α} positions in the α-helices between single monomers is less than 0.2 Å. As there is virtually no difference between the rRMPK and 1PKN structures, the rRMPK structure was used to compare with the S402P M_1-PK structure. The first 11 residues are not visible in either the rRMPK or the S402P M_1-PK electron-density maps. These same residues are also not visible in the 1PKN structure.[17]

Analysis of the S402P M_1-PK crystallographic data shows that a specific single mutation in the monomer increases the flexibility and dynamics of the tetramer. Attempts to model the S402P M_1-PK structure with 8-fold symmetry failed, primarily because there is an increase in the conformational variability of the B domain and an increase in the dynamic behavior of the 399-407 loop regions.

To determine the optimal refinement procedure for the S402P PK data, various non-crystallographic, symmetry-averaging models were tested at the same step. The results indicate that the S402P M_1-PK is best modeled using 2-fold, non-crystallographic symmetry refinement (identical tetramers; Table 1). The *R*-factor and R_{free} convergence of the refinement at 2.8 Å are 0.239 and 0.273, respectively, as shown in Table 2. The initial electron density maps were readily interpretable in one region of the asymmetric unit, but unclear in the 2-fold non-crystallographic symmetry-related region. The density averaging technique iteratively averages the electron density across the non-crystallographic symmetry elements until the phase angles converge. In this study the 2-fold density averaging improves the phases and yields electron-density maps that are clearer and interpretable. This conclusion is illustrated by the analysis of the region defined by residues 126 to 132. In the 1PKN structure, residues 126-130 could not be modeled because there was insufficient electron density in that region of the map. The unaveraged electron density map of the S402P structure is largely discontinuous and uninterpretable. Following 2-fold density averaging, the electron density around residues 126-130 in the S402P structure is nearly continuous and interpretable. The final *R*-factor

Table 1. Effect of non-crystallographic symmetry density averaging on refinement of the S402P structure

	NCS symmetry (N-fold)	R_{free}	*R*-factor
Octomer	1	0.345	0.208
Tetramer	2	0.313	0.237
Dimer 1,2	4	0.336	0.285
Dimer 1,3	4	0.314	0.266
Monomer	8	0.308	0.278

Table 2. Refinement results

A. *S402P structure*				
R_{free} (# reflections)	0.273 (9149)			
R-factor (# reflections)	0.239 (83018)			
Number of non-hydrogen atoms/tetramer	15936			
Number of water molecules/tetramer	102			
rms (bond distances in Å)	0.008			
rms (bond angles in deg.)	1.3			
Estimated coordinate error (Luzzati)	0.38 Å			
Average *B*-factors/tetramer	38.3 Å^2			
Domain A	31.7 Å^2			
Domain B	56.5 Å^2			
Domain C	36.9 Å^2			
Domain N	32.1 Å^2			
Waters	29.5 Å^2			
Ramachandran plot (PROCHECK)	1	2	3	4
Most favored	390 (85.2 %)	397 (86.7 %)	396 (86.5 %)	392 (85.6 %)
Allowed	60 (13.1 %)	56 (12.2 %)	58 (12.7 %)	56 (12.2 %)
Generously allowed	4 (0.9 %)	2 (0.4 %)	2 (0.4 %)	4 (0.9 %)
Disallowed	4 (0.9 %)	3 (0.7 %)	2 (0.4 %)	6 (1.3 %)
B. *rRMPK structure*				
R_{free} (# reflections)	0.247 (7985)			
R-factor (# reflections)	0.239 (71333)			
Number of non-hydrogen atoms/ monomer	3984			
Number of water molecules	0			
rms (bond distances in Å)	0.007			
rms (bond angles in deg.)	1.3			
Estimated coordinate error (Luzzati)	0.39 Å			
Average *B*-factors/monomer	48.0 Å^2			
Domain A	38.4 Å^2			
Domain B	81.4 Å^2			
Domain C	40.5 Å^2			
Domain N	38.6 Å^2			
Ramachandran plot (PROCHECK)	1			
Most favored	397 (86.5 %)			
Allowed	57 (12.4 %)			
Generously allowed	4 (0.9 %)			
Disallowed	1 (0.2 %)			

overall from map averaging was 0.113 with an operator correlation coefficient of 0.963. There are 102 ordered water molecules included in the S402P M_1-PK structure. The 126-132 loop is the most dynamic region of the protein with residues 128 and 129 sometimes in the generously allowed region of the Ramachandran plot.

Monomer conformation

Comparison of domain-domain and monomer-monomer orientations in the S402P M_1-PK structure to all available rabbit muscle PK structures, rRMPK (this study), 1PKN,[17] 1AQF,[18] 1A5U[19] demonstrates that, within a few percent, these structures adopt a similar tertiary and quaternary alignment. The least squares alignment of the C^α positions in the α-helices between the four monomers of the S402P M_1-PK and the single rRMPK monomer structure are ca 0.2 Å rmsd, indicating an overall agreement in the peptide backbone positions of the helices. Significant differences between the S402P M_1-PK and rRMPK structures are seen in the loop containing the site of mutation, the dynamic loops of the B domain and the putative FBP binding region[20] near the C terminus (Figure 2). The rmsd values of the C^α positions are greater than 1.5 Å in the 401-406 loop, greater than 1.9 Å in the 120-154 loop in the B domain, and greater than 0.9 Å in the putative FBP binding region. A comparison of all of the known PK structures shows a similar arrangement of the α-helices in the monomers. Least squares alignment of the C^α positions in the α-helices of the monomers of the known PK structures against the monomer of the S402P M_1-PK structure, results in rmsd values of <0.1 Å, well within experimental error. Thus, any structural differences between the PK structures will be manifested in the non-α-helical portions.

Further observation, using the procedure outlined by Gerstein,[21] reveals that, in addition to similarities in the higher-order structure, the relative orientation of the 17 helices (as defined in the 1PKN structure) show high similarity within each monomer of all available rabbit muscle PK structures, as well as the yeast,[20] *Leishmania mexicana*[22] and *Escherichia coli*[23] enzymes.

B domain

Domain B is a very flexible region of the monomer of PK. The *B*-factors of the B domains of the S402P M1-PK and rRMPK structures are signifi-

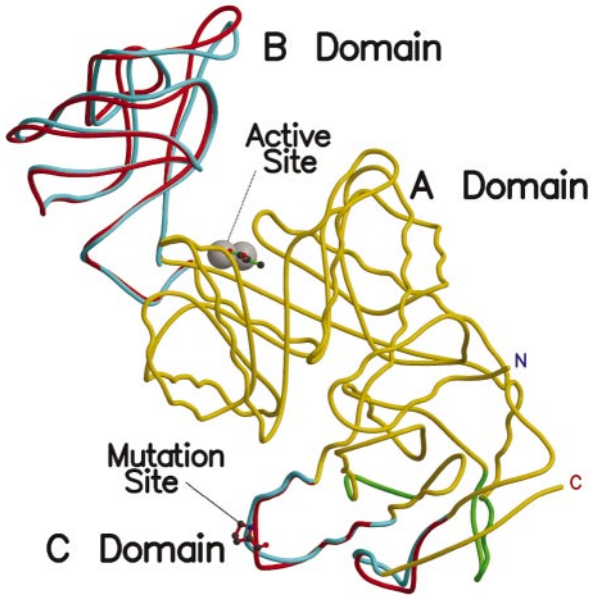

Figure 2. View showing the superposition of the rRMPK structure (cyan) on the S402P structure (red). The regions where the chains exactly superimpose on each other, within experimental error, are shown in yellow. The major differences are in the B domain, the loop containing the S402P mutation site (C Domain) and the putative FBP binding loop, shown in green.

cantly higher than the other domains (Table 2). Previously published PK crystal structures also show the dynamic nature of the B domain with high *B*-factors and different residue rotational conformations. The 1AQF structure, which is the co-crystal of the pseudo-substrate phospho-lactate and wild-type M_1-PK, can be modeled with seven of its eight monomers in either of two rotational conformations of the B domain and the other monomer with its B domain density not visible.[18] The 1PKN structure has large *B*-factors (ca 100 Å^2) for its B domain with areas of weak density that required the modeling of several side-chains as methyl groups and the omission of residues 127-131 from the model.

In a general sense, residues 126-130 in the S402P M_1-PK structure adopt conformations similar to those seen in both the open and closed configurations between the A and B domains found in the 1AQF structures (Figure 2). The B domain is capable of rotating away from the A domain generating the open configuration. The amount of rotation of the B domain varies from 11° to 41°. Residues 126-130 of the B domain constitute the most dynamic region, which is probably stabilized upon binding of the reactants to the A domain during catalysis.[18] The B domain of monomer 1 in the S402P M_1-PK structure adopts the conformation of the closed form of the B domain, as observed in monomer 1 in the 1AQF and the rRMPK structure of this study. That is, this region extends down toward the A domain. Monomers 2, 3 and 4 show the 126-130 region extending away from the A domain.

The conformational flexibility of the B domain in the S402P M_1-PK structure was investigated by a rigid-body refinement procedure that allows the B domain of each monomer to move independently about residues 116 and 223 as the hinge points. The refinement revealed that there was up to a 3° variation in the domain rotation for the eight monomers. A similar rigid-body refinement was performed using the rRMPK data, which showed identical rotation angles between the B and A domains.

Putative FBP binding site

The putative FBP binding site for S402P, as suggested from the yeast PK (YPK) structure with bound FBP,[20] is situated between the residues preceding helix 15 (residues 428-434) and the loop comprised of residues 512-520 (Figure 3). Binding of FBP to the YPK was shown to order the residues of the yeast enzyme, which are equivalent to residues of 475-480 and 512-520 in the S402P structure. There is no disorder of these residues in the S402P structure. This relatively higher structural order in the absence of bound FBP implies that this region in the S402P M_1-PK structure is less dynamic than the comparable region in the yeast structure.

In the putative FBP binding site of the S402P structure, threonine 431 and serine 436 form hydrogen bonds to a water molecule. Glutamate 432 and arginine 454 coordinate to another water molecule that is located 9.9 Å from the other water molecule. This distance is comparable with the distance from one end of the FBP molecule (03P) to the other (05P). A manual fit of the FBP molecule from the yeast structure shows that the FBP molecule can fit in the S402P putative FBP binding site with the 03P and the 05P atoms placed in the locations occupied by the two water molecules.

Unlike the yeast structure, the 512-520 loop of the mammalian structures is positioned close to the C terminus of helix 17. The side-chain of tryptophan 481 is rotated relative to the yeast equivalent tryptophan to allow the 512-520 loop to approach helix 17. The 512-520 loop of the S402P structure does not approach as close to the C terminus of helix 17 as the equivalent loop in the 1PKN, the rRMPK and the *L. mexicana* structures. However, its conformation is shifted towards the position exemplified by the yeast structure (Figure 4). It should be noted that although the apex of the 512-520 equivalent loop in the *L. mexicana* structure is close to the C terminus of helix 17, its overall conformation is quite different from the mammalian structures. The 512-520 equivalent loop of the *L. mexicana* structure is twisted between residues 480 (512 in rRMPK) and 489 (521 in rRMPK) along the axis between the β21 and β22 pleated sheets. This arrangement covers the puta-

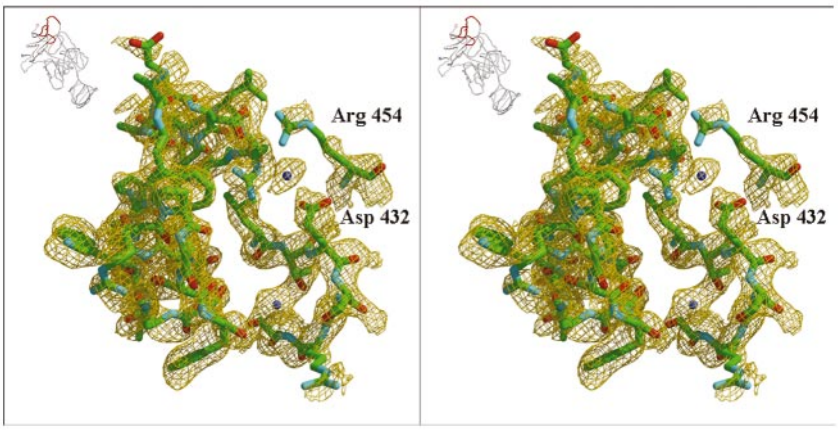

Figure 3. Stereo view of the putative FBP binding region of the S402P structure. The inset shows the location of the FBP binding region (red) in the monomer. Shown are residues 430-436, 454, 480-489 and 510-520. Contours are at 1 σ. The two water molecules (blue spheres) closely coincide with the positions of the phosphate oxygen atoms of the FBP molecule as seen in the yeast enzyme. Arginine 454 interacts with the water molecule and glutamate 432, which also interacts with the water molecule.

tive FBP binding site, and causes a shift of the area where the FBP could bind.[22] In addition, the N terminus of helix 17 is shortened in the *L. mexicana* structure, and the course of the polypeptide chain between residues 443 (475 in rRMPK) and 453 (485 in rRMPK) is quite different from the S402P and the other mammalian structures. Lys453 is postulated to form the contact with the FBP. In the S402P structure, residue 453 is a valine residue, and is in the middle of helix 17 and cannot interact with a FBP molecule. However, the Arg454 of the S402P structure is positioned to possibly bind to FBP.

The active site

Comparing the active-site orientations in the four monomers of the S402P M_1-PK and the monomer of the M_1-PK structure reveals the high degree of similarity in each of the subunits. The Ramachandran plot shows that the refined S402P M_1-PK structure possesses a reasonable geometry (Table 2) with more than 99 % of ϕ-ψ angles in the allowed regions. In all monomers Thr327 is found near or in the unallowed region. This allows Thr327 to strongly coordinate to the pyruvate in the active site. The arrangement of the active-site atoms of monomer 1 differs from that of the other three monomers of the tetramer. Monomer 1 does not

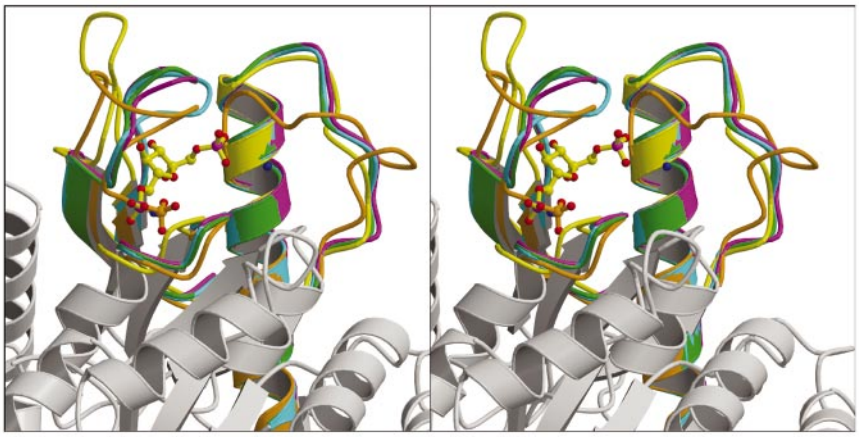

Figure 4. Stereo view of the FBP binding region of the yeast enzyme (yellow) with the RMPK (magenta), rRMPK (cyan), S402P (green) and the *L. mexicana* (orange) structures superimposed by least-squares fitting of helix 17 (multicolored) of the four structures. The courses of the polypeptide chains of the structures between residues 475 and 485 (rRMPK numbering) are shown on the upper-right of the figure. The FBP of the yeast structure (yellow carbon atoms), the sulfate from the *L. mexicana* structure (sulfur, orange) and the water molecules (oxygen, blue) from the S402P structure are also shown. The remainder of the S402P structure is shown in gray.

have water molecules coordinating to the metal ions (Figure 5(a)). However, monomers 2, 3 and 4 show a water molecule participating in the octahedral coordination of the Mn^{2+} ion and another water molecule coordinating to the K^+ ion (Figure 5(b)).

The orientation of the side-chain of Ser242 of monomer 1 differs from the orientation in monomers 2, 3 and 4 in the S402P M_1-PK structure. In monomer 1 the hydroxyl group of Ser242 is oriented towards Glu271, forming a hydrogen bond with the free O^{ε} atom in a manner that would allow hydrogen bonding to a water molecule that would be expected to occupy the last of the octahedral coordination sites (Figure 5(a)). It is of interest to note that in the yeast structure with bound FBP the hydroxyl group of the equivalent serine is oriented in the same manner. The other three monomers of the S402P M_1-PK structure have the Ser242 hydroxyls oriented toward the K^+ which, albeit distant (~3.6 Å), may play a role in ion coordination (Figure 5(b)).

Site of S402P mutation

Molecular dynamic calculations involving the alternative splicing region of the M_1/M_2 sequence (residues 388-423) indicate that the type of residue at the 402 position is important in determining the backbone orientation of the residues 399-407 loop.[10] This loop is located between the helices involved in the pseudo-four-helical bundle Y interface. The *B*-factors of the published M_1-PK structures show this loop region to be highly dynamic even though it is firmly tethered by its neighboring helices. The loop regions of the monomers of S402P M_1-PK also exhibit high *B*-factors. The backbone conformation of the loop region varies for each monomer (Figure 6). The general conformation of this variable region is closer to the corresponding loop in the allosteric form of YPK, which also has a proline at the corresponding 402 position. The proline residue substitution has a large effect on the ϕ-ψ angles of residues 400 and 401. The substitution kinks the backbone of the loop away from the C domain of the adjacent subunit (as much as 2 Å) creating an altered van der Waals packing and a different hydrogen bond network (Figure 7(a) and (b)).

The start of the wild-type M_1-PK 399-407 loop is apparently stabilized by the hydrogen bonds of the side-chains of Ser401 and Ser402 to the peptide carbonyl oxygen atoms of Leu397 and Arg399, respectively, and the hydrogen bond between Glu409 and Ser404. In the S402P M_1-PK structure the carbonyl oxygen atom of Pro402 participates in hydrogen bonding and alters the loop conformations. A different set of interactions stabilizes the loop region that, as evident from its dynamic nature, apparently allows easy inter-conversion between the observed conformations (Figure 7(a) and (b)). The S402P M_1-PK structure shows that the Ser401 O^{γ} atom can reach either the Leu397 or Arg398 backbone. Furthermore, the Ser401 O^{γ} atom is positioned so that it can interact with either the N^{ζ} atom of Lys421 of the opposing monomer or the carbonyl oxygen atom of Leu397.

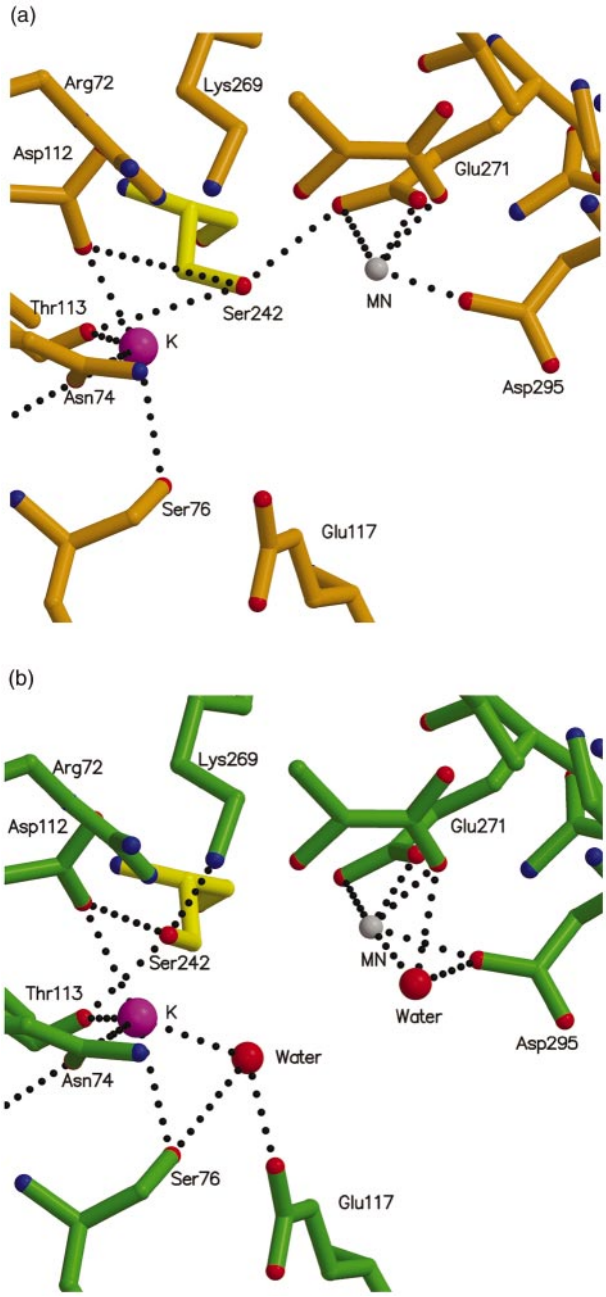

Figure 5. (a) View of the active site of monomer 1 (orange) of the S402P structure showing the O^{γ} atom of Ser 242 (yellow) directed toward the O^{ε} atom of Glu271. Broken lines indicate hydrogen bonds. (b) View as in (a) showing the O^{γ} atom of Ser242 (yellow) in monomer 2 (green) directed toward the O atom of Thr113 and N^{ζ} atom of Lys269. Note also the addition of a water molecule interacting with Ser76, Glu117 and the K^+. A second water molecule is interacting with Asp295, pyruvate residue and the Mn^{2+}.

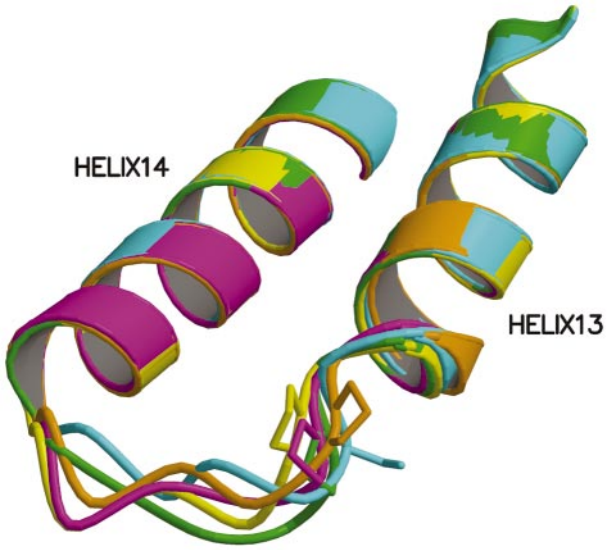

Figure 6. View of the C^{α} positions of residues 391-406 containing the S402P mutation site between helix 13 (residues 390-400) and helix 14 (residues 407-421). The structures of monomer 1 (orange), monomer 3 (yellow), monomer 4 (magenta), and rRMPK (cyan) are shown superimposed on monomer 2 (green). The regions of helices 13 and 14 are included to illustrate the high degree of conformational identity inherent in the structures.

In monomer 1, the hydrogen bond between the O^{γ} atom of Ser401 and the N^{ζ} atom of Lys421 of the opposing monomer 2 limits the proline induced loop protrusion into the Y interface found in the other three monomers. The absence of detectable hydrogen bonds in the residues 400-405 of monomer 3 are consistent with this loop having the largest conformational deviation, and gauged from its *B*-factors, the lowest stability.

Alteration in the backbone conformations of the S402P loops occurs with different sets of hydrogen bonds to the negatively charged residues lining the cavity. The loop residues Asp406 and Glu409 enter into a hydrogen bond network with residues Gln439, Arg442, Tyr443, and the water molecule found near Glu409. The rRMPK structure shows the side-chain of Asp406 directed into the solvent and the side-chain of Glu409 oriented toward the 399-407 loop, allowing the formation of hydrogen bonds with Ser404 and possibly Lys421. The S402P M_1-PK structure has both residues 406 and 409 oriented into the cavity and entering into hydrogen bonds. The extent of contact varies amongst the four monomers. One carboxyl oxygen atom of Glu409 in monomer 1 forms hydrogen bonds with the hydroxyl group of Tyr443 and one hydrogen bond to Arg442 and a water molecule. Monomers 2, 3, and 4 have one Glu409-Tyr443, one Glu409-Lys421, one Glu409-Arg442 and one Glu409-Water hydrogen bond.

Dimer interface

There are two interfaces (Figure 1(b)) in the PK tetramer.[5,17] The Y interface involves the C and N domains of monomers 1 and 2 and monomers 3 and 4. The Z interface is approximately perpendicular to the Y interface, and involves all four domains between monomer pairs 1-3 and 2-4. Surface area calculations reveal that less surface is buried between the 1 and 2 monomers, the Y interface (2813 $Å^2$), than between the 1 and 3 monomers, the Z interface (5945 $Å^2$). This supports the proposal that dissociation of the tetramer into dimers would occur at the Y interface.[16] The tetramer possesses approximate 222 symmetry with the largest deviation of 3° at the Z interface.

The 1 and 2 monomers align the respective C domains in a ''tail-to-tail'' fashion (Figure 1(b)). Helices 13 and 14 form a helix-loop-helix region (residues 390 to 421) in the C domain, which interacts in a pseudo-four-helical bundle with its counterpart in the opposing monomer (Figure 8). This helix-loop-helix region, which includes residue 402, is in the alternatively spliced region of the M_1/M_2 encoded RNA, and must therefore carry information for conferring allosteric regulation. A particularly prominent feature in this region is Lys421, which protrudes across the Y interface into, and through, the loop between helices 13 and 14. The 399-407 loop creates a cavity in the protein that has a negative electrostatic-potential into which the Lys421 of the opposing monomer protrudes. The Lys421 interacts with several residues in the opposing monomer, notably Glu409 and Tyr443 (Figure 7(a) and (b)). Lys421 has been implicated as an essential residue in inter-subunit communication.[10] Several altered side-chain conformations are also found within the N domain in the cavity formed at the junction of the four monomers. Residues 389, 391, 399 adopt conformations that are either oriented into the solvent (including refined water molecules) or produce no detectable alterations or new interactions.

The Z interface encompasses extensive contacts between the adjacent A domains with minor contacts with the B and N domains (Figures 1(b) and 8). This interface also contains residues that flank the opening to the active site, which have been proposed to contribute to the stabilization of the active form of the enzyme.[23] The main interactions are an inter-subunit crossing of helix 11 (residues 341-353) and the bulging portion of helix 10 (residues 302-319) into the first 34 amino acid residues of the N terminus and the top half of helix 12 (residues 368-378) of the opposing monomer. Helix 12 spans both interfaces and extends into the active site. The relative orientation of the monomers, the interacting helices, and the general positioning of the side-chains are very similar between the S402P M_1-PK and rRMPK structures.

Another key feature of the Z interface is a salt-bridge near the opening of the active site between the invariant residues Arg341 and Asp177 in the

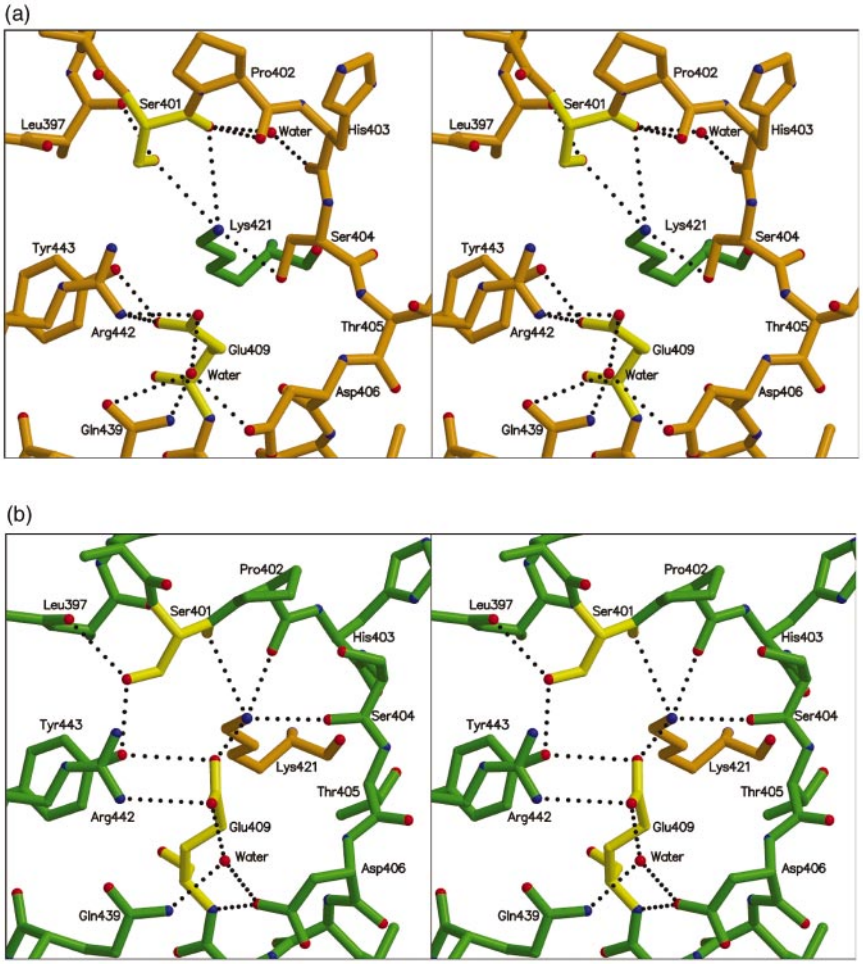

Figure 7. (a) Stereo view of the helix 13-loop-helix 14 site of monomer 1 (orange) with Lys421 of monomer 2 (green) protruding into the loop. Note the conformations of the side-chains of Ser401 and Glu409 (yellow) which are as found in the T state structures. (b) Stereo view of the helix 13-loop-helix 14 site of monomer 2 (green) with Lys421 of monomer 1 (orange) protruding into the loop. The conformations of the side-chains of Ser401 and Glu409 (yellow) differ from monomer 1 and are as found in the R-state structures.

opposing A and B domains, respectively (Figure 9). It is interesting to note that this interaction is disrupted in the S402P M_1-PK structure (Figure 10). The side-chain of Asp177 is instead reoriented toward the active site of the same subunit. The χ_1, and χ_2 angles of Asp177 of all of the S402P M_1-PK monomers are similar to those found in the *E. coli* structure, which is proposed to be in the T form.[9]

The position of the Arg341 side-chain remains relatively unchanged with either a slight movement back toward the backbone as in monomers 1 and 2, (where it hydrogen bonds with the carbonyl oxygen atom of Gly294 from the opposing monomer) or with a tilt, as in monomer 3, which brings the N^{η} atom closer to the carbonyl oxygen atom of Pro339. It also appears that there is a loss of the hydrogen bond between the Arg338 N^{η} atom and Gly297. The side-chain of Arg338 swings ~50° into the solvent and does not appear to make any specific interactions. Concurrent with the loss of the 177-341 salt-bridge and the 338-297 hydrogen bond in the S402P M_1-PK structure is an apparent increase in the rotation of the B domain about the hinge point as discussed in ''B Domain''.

Another interesting perturbation of the intersubunit interactions involves Phe25. The S402P structure differs from the wild-type M_1-PK (1PKN) with an additional inter-monomeric interaction involving the aromatic rings of Phe25 (Figure 11). The Phe25 residues in the S402P M_1-PK have χ_1 and χ_2 dihedral angles of −85° and 74°, respectively; as opposed to the 1PKN values of −180° and 36°. The rings of the S402P Phe25 are oriented with the C^{γ} atom of one ring almost over the C^{ζ} atom of the ring of the opposing monomer across the Z interface (Figure 1(b)). The inter-planar distance is ~3.6 Å, which is slightly greater than the minimal distance for ring-ring interactions.[24–26] Changing the orientation of the Phe25 rings to the edge to face interactions observed in the 1PKN structure, followed by energy refinement, resulted in the rings resuming the face-to-face orientation with the ring plane normals making an angle of ~8°. The Phe25 interactions of the S402P M_1-PK structure

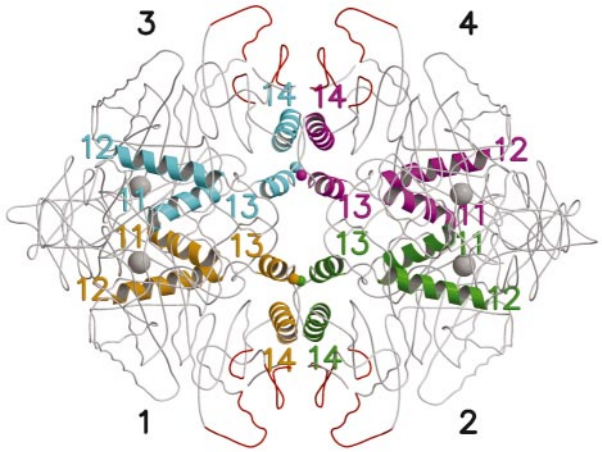

Figure 8. View as in Figure 1(b) showing the locations of helices 11-14. Colors of helices refer to their respective monomer. The gray spheres indicate the location of the active site. The putative FBP binding region of the S402P structure is shown in red.

are very nearly a true face-to-face orientation with the rings arranged in a head-to-tail fashion placing the C^{γ} atom over the C^{ζ} atom of the opposing ring. The Phe25 ring orientation of the rRMPK structure is nearly identical with the S402P structure (Figure 11). In the other known non-mammalian PK structures, the equivalent residue at position 25 is either not present, as in *E. coli*, is a glutamine residue, as in *L. mexicana*, or is an arginine residue, as in yeast. None of these residues interact across the Z interface. The significance of this association of phenylalanine rings across the monomer-monomer interface of the structures of the recombinant proteins is unclear and awaits further investigation.

Discussion

Allostery is a mechanism employed in the regulation of metabolism, intercellular communication, gene expression and other cellular functions. One of the major issues on allostery is the mechanism of signal transmission. What are the pathways of signal transmission? Is there a specific pathway designed for the allosteric enzyme to transmit the signal from an effector site to the functional site? Is there a separate pathway for each different effector? How is a signal transmitted across a subunit interface? Could it be possible that there is no specific pathway, and the whole subunit participates in signal transmission? This issue of global *versus* specific pathway is a central question that has not been definitively answered. However, results from a computational chemistry study indicate that the communication between binding sites can be represented by a shift in the distribution of the conformational ensemble.[27] Results of this study, as summarized in Table 3, are consistent with the concept that PK exists as ensembles of conformational states that can be observed even in crystalline states in the form of micro-heterogeneity in the rotational flexibility of the B domain.

In mammalian PK, it is shown that imparting effector susceptibility to this enzyme can be as simple as a single amino acid residue substitution,[10,28,29] or even the removal of a hydroxyl group.[10] The S402P mutation led to two functional changes in M_1-PK, namely, an enhanced sensitivity to phenylalanine inhibition and a decreased responsiveness to FBP activation. These functional alterations may be the consequences of perturbations at the binding sites of these effectors or changing of the equilibrium constant governing the distribution between the active R, and inactive, T-state of PK or both. This study shows that a consequence of the S402P mutation involves a change in the dynamics of multiple loci in the protein. The S402P M_1-PK structure shows that the stability of the loop region between helices 13 and 14 (Figure 8) and the inter-subunit, inter-domain salt-bridge between Arg341 and Asp177 (Figure 9) are certainly disrupted. Compared with the wild-type M_1 structure, the B domain can assume an increased manifold of positions with respect to the A domain. In the S402P M_1-PK structure the side-chain of Asp177 is turned away from Arg341 of the adjacent subunit and towards the active site. The χ_1 angles of Asp177 of all four monomers are similar to those of the *E. coli* (T form of the enzyme).[9,23] There are no direct protein contacts made with the side-chain of Asp177. Breaking of the Asp177-Arg341 salt-bridge does not appear to have as large an effect at the Arg341 site. No rearrangement of helix 11, in which Arg341 resides, is observed. There are minor side-chain movements at Arg341 that culminate in new

Table 3. Summary of structural perturbations by the S402P mutation

Site	Perturbation
Active site	Alternate orientations of some residues in different monomer.
Y Interface	Alternate conformations of the loop that contains residue 402; alternate inter-subunit interaction involving residue 406.
Z Interface	Breaking of inter-domain, inter-subunit salt-bridge; alternate conformational state of Phe25.
B Domain	Increase in rotational flexibility.

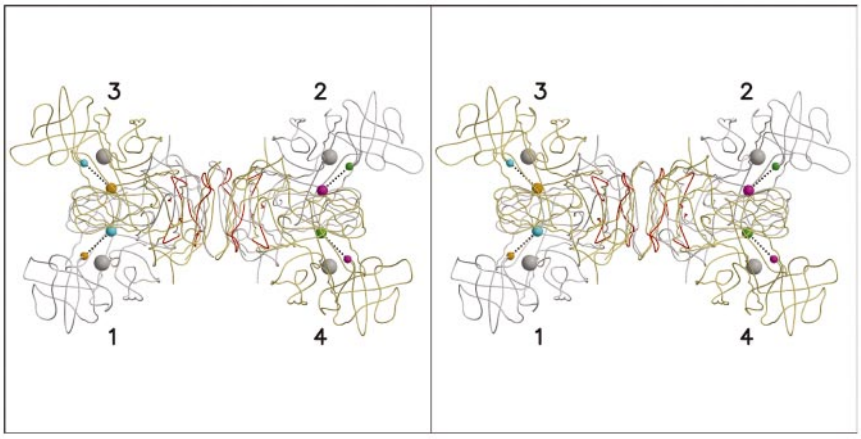

Figure 9. Stereo view as in Figure 1(b) rotated 90° around the horizontal axis showing the locations of the salt-bridges across the Z interface between Asp 177 (small colored spheres) of one monomer and Arg 341 (larger spheres) of the other monomer. Colors of spheres refer to their respective monomer. Large gray spheres indicate the location of the active site. The putative FBP binding region of the S402P structure is shown in red. Monomers 1 and 2 are lightly colored to distinguish them from monomers 3 and 4.

hydrogen bonds with the carbonyl oxygen atom of Gly294 (from the opposing monomer) or carbonyl oxygen atom of Pro399. The side-chain of Arg338 swings (~50°) into the solvent, thereby losing its hydrogen bond to Gly297. Concurrent with the loss of the Asp177-Arg341 salt-bridge in the S402P M_1-PK structure is an apparent increase in the freedom of rotation of the B domain about the hinge point. Rigid-body refinement of the B domain produced a variation of up to 3° in rotation for all monomers. Similar refinement of the rRMPK structure, which retains the Asp177-Arg341 salt-bridge, shows essentially no difference in the rotation in seven of the eight monomers. This apparent correlation between salt-bridge formation and freedom of rotation of the B domain is a logical consequence of the fact that the bridge is formed between the B and A domains of adjacent subunits. Formation of the inter-domain salt-bridge is expected to anchor the movements of the B domain.

Previously published rabbit muscle structures, containing different ligands, also demonstrates the relation between the presence of the Asp177-Arg341 salt-bridge and the rotational flexibility of their B domain. The first rabbit muscle PK structure solved by Larsen *et al.*[17] (1PKN) was crystallized under conditions similar to those employed for S402P M_1-PK and rRMPK. These conditions include the presence of pyruvate, K^+ and Mn^{2+}. The 1PKN structure is found to maintain the salt-bridge. The 1PKN structure was refined using a monomer with 8-fold, non-crystallographic symmetry (two tetramers in the asymmetric unit). The *B*-factors for the B domain are high but the structure was refined to an *R*-factor of 22%, indicating sufficient uniformity of monomer conformations to model the eight B domains as one conformation. Thus, in the 1PKN and rRMPK structures the presence of the salt-bridge is correlated with uniformity of the B domain rotational conformation.

In another study of M_1-PK that was crystallized in the presence of the pseudo-substrate L-phospholactate and the counterions Mn^{2+} and K^+, the structure was refined with three different orientations of the B domain within the two tetramers in the asymmetric unit.[18] Six of the monomers show the B domain in the open conformation and one in the closed conformation. One B domain was not resolved due to extensive disorder. In each of the seven resolved B domains the Asp177 is oriented away from the Arg341, and does not form the salt-bridge. Only in the closed B domain is the side-chain of Asp177 oriented towards the active site. It does not, however, enter into the network of the substrates or protein. Hence, in this structure the absence of the salt-bridge is related to an increase in the number of conformations assumed by the B domain, and all of them assume an open conformation, the conformation proposed by Consler *et al.*[8] and Mattevi *et al.*[9] as the inactive T-form. Thus, a breakage of the salt-bridge apparently shifts the state equilibrium constant in favor of the inactive T-state.

The deepest penetration of the side-chain of Asp177 into the active site is found with M_1-PK complexed with Mg^{2+}-ATP-Na^+-oxalate (1A5U).[19] Of the eight subunits found in the unit cell (two tetramers) six were fully liganded and two were missing the ATP. Large conformational changes were observed in the orientation of the B domain, and no subunit maintained the Asp177-Arg341 interaction. The B domains of those monomers with the ATP bound moved closer to the A domain and the Asp177 penetrated to within ~4 Å of the Mg^{2+}-ATP. Thus, once again a correlation can be established in this structure between the

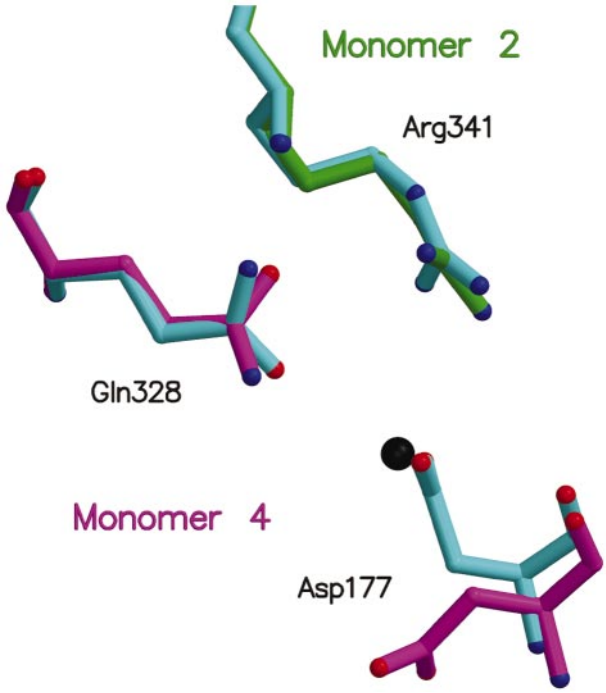

Figure 10. View of the Asp177-Arg341 inter-monomer salt-bridge, with Gln328. Residues 177, 328 and 341 of the S402P structure are shown (magenta and green) with the corresponding residues of the superimposed rRMPK structure (cyan). The fit is quite good, except for the side-chains of the Asp177 residues. The carboxyl group of Asp177 of the S402P structure (magenta) points toward the active site. Whereas, the Asp177 of the superimposed rRMPK structure (cyan) points toward the Gln328 of the same monomer and toward the Arg341 of the opposite monomer. In the S402P structure, a water molecule (black sphere) occupies the space where the carboxyl moiety of Asp177 is situated in the rRMPK structure.

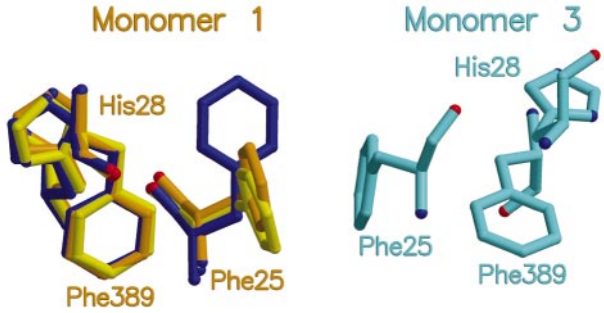

Figure 11. View of the Phe25-Phe25 interaction in the S402P structure (orange and cyan). The residues from the rRMPK structure (yellow) and the 1PKN structure (blue) are also shown. See the text for details.

disruption of the salt-bridge and a change in the orientation of the B domain.

In addition to mammalian PK, a similar pattern of structural linkage between the formation of the salt-bridge and dynamics in domain rotation is reported in YPK.[20] Structure of YPK in the presence and absence of the effector FBP (1A3W and 1A3X, respectively) were determined. In both tetrameric structures the Asp177-Arg341 salt-bridge (Asp147-Arg314 in the yeast sequence) is intact. Refinement of the structures was successful by employing non-crystallographic symmetry, i.e. tetramer refinement using just one monomer. The quality of the refined structures implies that all four subunits had the same B domain orientation. Inspection of YPK without FBP shows that even though the B domain of the two monomers in the unit cell (monoclinic *C*2) differ in rotation by about 4°, they maintain the salt-bridge. In summary, all the available structural information on PK indicates a linkage between the dynamics in the rotational state of the B domain with the presence of the Asp177-Arg341 salt-bridge. An increase in domain rotational freedom is apparently associated with the absence of the salt-bridge.

The relationship for B-domain stability and the Asp177-Arg341 salt-bridge as seen in the muscle PK crystal structures also can be supported from genetic observations. Using information derived from genetic evidence based on studies of erythrocyte PK in hereditary non-spherocytic hemolytic patients, mammalian PK mutants at residues 340 were generated. Studies revealed that the mutation at the 340 residue, threonine to methionine residue, is detrimental to the function of PK.[11–13] The structural effects (i.e. impediment of the Asp177-Arg341 salt-bridge) of the T340M PK mutants have not been determined. Kinetic analysis of T340M M_1 and M_2-PK mutants revealed alterations in steady-state behavior similar to those found in the S402P M_1-PK mutant. The mutation produces significantly reduced enzyme activity, indicated by a decrease in the K_{cat} and an increase in $K_{m,app}$ for PEP in the presence of 2 mM ADP. This result indicates a communication between residue 402 and the active site, which resides about 40 Å apart. No change in the $K_{m,app}$ for ADP is observed. In addition, the T340M mutation effects a significant enhancement in the association behavior at the Y interface, site of the residue 402. In other words, a mutation at one interface affects the association pattern at another interface 40 Å away. These results establish the functional linkage between these two regions, the loop between helices 13 and 14 and the turn at the beginning of helix 11 which contains residue 340. This structural study identifies the nature of changes in those two regions. Thus, both structural and functional studies lead to a consistent conclusion in revealing the linkage of these regions in the allosteric regulation of PK.

Having established the correlation between the formation of the Asp177-Arg341 salt-bridge and rotational motion of the B domain, it is important to define the functional relevance of these structur-

al changes. Based on small angle neutron scattering data, Consler *et al.*[8] proposed that the inactive, T-state can be represented by a rotation of the B-domain in opening of the cleft between the B and A domains. A closing of the cleft can represent the active, R-state. The increased dynamic of the B domain in the S402P M_1-PK is consistent with a change in the equilibrium constant governing the distribution of R and T-states most likely towards the T-state. It is, therefore, not surprising that the S402P mutation leads to an increase in sensitivity to phenylalanine, the binding of which shifts the equilibrium towards the T-state. The decreased responsiveness to FBP and lower apparent affinity for PEP are also consistent with the interpretation that the S402P mutation favors the distribution towards the T-state. By comparing the structures of the rabbit muscle (1PKN) and *E. coli* PK, Mattevi *et al.*[9] noticed the presence and absence of the Asp177-Arg341 salt-bridge, respectively. As the structures of the mammalian and *E. coli* PK are interpreted as representative of R and T-state, respectively, it was proposed that Asp177 plays an important role in the T ⇆ R transition.

In a recent study of the structure of PK from *L. mexicana*, it was shown that the region containing residue 341 is in a more dynamic state when the enzyme assumes the inactive T-state.[22] It was further reported that there is significant loop dynamics in the effector binding site. In conjunction with this study, it seems that an increase in dynamics in specific loci in the protein structure is correlated with the conferring of allostery in PK. Hence, a consistent structure-function correlation is emerging. It is most encouraging that the strategy of combining human genetic information with solution biophysical and structural studies is yielding consistent information to elucidate the molecular mechanism of allosteric regulation in PK.

Concluding Remarks

Results from the literature and this study indicate the importance of the formation of the inter-subunit and inter-domain salt-bridge between Asp177 and Arg341 in defining the distribution of the PK conformation between the R and T-states. These conformations are intimately linked to the movement of the B domain towards or away from the A domain. It is not surprising to observe an increase in the freedom of the B domain for rotation with a breakage of the salt-bridge, because this interaction is inter-domain in nature. Furthermore, nature's selection of this particular salt-bridge is logical. Formation of this inter-domain salt-bridge anchors the B domain to the A domain *via* Arg341, which is highly connected to the active-site residues.[30] As this salt-bridge also constitutes an inter-subunit interaction between two domains of adjacent subunits, it is not surprising that the consequences of transmission of information through this particular structural element are global in nature. It seems that allosteric proteins might be engineered to have clusters of structural elements that are highly connected in a manner analogous to the pattern of inter-molecular interactions observed in cells.[31]

There is ample evidence in this study to indicate that PK can exist in ensembles of microstates, namely, the various numbers of microstates observed in the active sites, rotational flexibility of the B domain and orientation of the Phe25 ring. Mutations or ligand bindings can perturb the distribution of these microstates.

Materials and Methods

Materials

Succinic acid, pyruvic acid, and Hepes were purchased from Sigma Biochemical and used without further purification. Polyethylene glycol 8000 was obtained from Fisher Scientific.

Overexpression and purification of rRMPK

Construction and expression of the S402P M_1-PK mutant and the wild-type rabbit muscle PK were as described.[10,11] The proteins were purified using the procedure described by Cheng *et al.*[11] FBP (0.4 mM) and dithiothreitol (0.2 mM) were added to all buffer solutions to enhance protein stability and reduce oxidative effects. Protein purity was estimated to be at least 95 % (w/v) from Coomassie blue staining of SDS-PAGE gels.

Crystallization conditions

The rRMPK and S402P M_1-PK enzymes were crystallized and processed under identical conditions. Prior to the crystallization process, approximately 2-3 mg of precipitated protein (2 mg/ml) was removed from the 70 % ammonium sulfate storage buffer and re-suspended in 200 μl of dialysis buffer (100 mM KCl, 10 mM Hepes (pH 6.0)). The solution was passed through a Superdex 200 HR 10/30 FPLC (Pharmacia) column at a flow rate of 1 ml/min for desalting purposes and as an additional purification step. Peak fractions were collected and dialyzed for four hours against one liter of dialysis buffer at 4 °C.

Crystallization of the proteins was achieved using the hanging drop method at ca 18 °C. The crystallization solution consisted of 2.9 mM sodium pyruvate, 1.2 mM $MnCl_2$, 0.45 M KCl, 30 mM succinate adjusted to pH 6.0, 9 to 11 % (w/v) polyethylene glycol 8000, and 1.5 mg/ml of protein. A stream of N_2 gas at 15 psi was bubbled into the wells before sealing to slow oxidation effects from the air. Crystals appeared in two to three days, and were fully formed in four to five days.

Data collection

X-ray data were collected using a MacScience DIP 2030H area detector mounted on a MacScience M06HF rotating anode X-ray generator running at 50 kV and 90 mA equipped with MAXOS optics. Crystals were soaked in solutions containing increasing glycerol concentrations ranging from 0.5 % to 20 % (w/v) in six steps. The crystals were flash-cooled using nitrogen boil-off from a Cryo Industries of America Cryo Cooler. Data sets con-

sisting of 400 one-half degree frames were collected from one crystal of each protein. The S402P M_1-PK PK and rRMPK crystals nominally diffracted to 2.33 and 3.0 Å resolution, respectively. Analysis of the S402P M_1-PK data collection statistics indicated that the resolution limit of useable data did not exceed 2.8 Å. No other crystal of S402P M_1-PK diffracted as well.

Data analysis and structure refinement

The diffraction images were integrated using the programs DENZO and SCALEPACK.[32] Data were later corrected as described by White *et al*.[33] Data collection statistics for the S402P M_1-PK and rRMPK crystals are summarized in Table 4.

Initial phases were obtained using the molecular replacement procedure of XPLOR[34]. The muscle PK structure,[17] PDB entry 1PKN, was used as the search model. Subunit and secondary structure numbering follow those described for 1PKN. Molecular replacement revealed the location of the two tetramers in the asymmetric unit. Subsequent refinement consisted of cycles of rigid-body positioning, positional minimization, *B*-factor optimization, density averaging and model building. Initial energy refinements were carried out using XPLOR with CNS used in the final steps.[34,35] Rigid-body refinements were performed using shells of increasing resolution (12-8 → 10-6 → 8-4 → 6-2.5 Å) with increasing numbers of rigid bodies in the order of tetramers, monomers, domains and then full positional refinement, with non-crystallographic symmetry applied between the domains. Non-crystallographic symmetry matrices obtained from the final rigid-body refinement were applied in all individual atomic refinements. Initially, strict 8-fold symmetry of one monomer was employed for both structures. The rRMPK structure was fully refined with strict 8-fold, non-crystallographic symmetry. However, it was determined during refinement that the S402P M_1-PK monomers did not adhere to strict 8-fold averaging. At the beginning of the refinement process, monomer 1 had been arbitrarily chosen for 8-fold, non-crystallographic symmetry averaging. Inspection of the subsequent 8-fold non-crystallographic symmetry averaged electron density maps indicated that several regions of the maps corresponding to monomers 2, 3 and 4 differed from monomer 1. Calculations using 1, 2, 4 and 8-fold, non-crystallographic symmetry averaging showed that 2-fold, non-crystallographic symmetry averaging gave better results (Table 1). Steadily improving refinement cycles using 2-fold, non-crystallographic symmetry averaging verified this conclusion (Figures 5 to 7). After the first round of modeling an anisotropic *B*-factor correction was made to the observed scattering factors. One cycle of simulated annealing was then carried out using XPLOR. Solvent flattening, individual atomic *B*-factors and positional refinement in CNS were used in final rounds of refinement. An additional round of simulated annealing was performed on the S402P M_1-PK structure when the non-crystallographic symmetry was reduced from 8 to 2-fold. Ordered water molecules were added to the S402P M_1-PK structure using the water-pick and delete function of CNS. Water molecules were kept if they were within hydrogen-bonding distance as determined by the contact protocol of employing distance, geometry and neighbor constraints. After each round of energy refinement $F_o - F_c$ and $2F_o - F_c$ electron-density maps were produced using a locally modified version of the density-averaging program RAVE.[36,37] The electron-density map chosen for model building was determined by calculating the rmsd of the phase angle from one cycle of RAVE to the next. When the phase angle converged, the electron-density map from that particular averaging cycle was chosen.

Table 4. Data collection statistics

S402P structure	
Space group	*P*1
Unit cell	$a = 82.1$ Å; $b = 108.7$ Å; $c = 144.4$ Å; $\alpha = 95.9°$; $\beta = 92.5°$; $\gamma = 111.7°$
Unique reflections	92,167
Resolution	90-2.8
R_{merge} (last shell)	0.132 (.256)
Redundancy (last shell)	1.6 (1.7)
Completeness (last shell)	81.8 % (79.2 %)
$I/\sigma(I)$ (last shell)	11.0 (4.2)
rRMPK structure	
Space group	*P*1
Unit cell	$a = 79.0$ Å; $b = 105.4$ Å; $c = 143.5$ Å; $\alpha = 95.9°$; $\beta = 92.8°$; $\gamma = 111.9°$
Unique reflections	79,318
Resolution	90-3.0
R_{merge} (last shell)	0.082 (.258)
Redundancy (last shell)	2.4 (2.2)
Completeness (last shell)	93.2 % (82.9 %)
$I/\sigma(I)$ (last shell)	9.1 (3.1)

Manual intervention

The energy-refined coordinates were manually fitted into averaged electron density maps using the program O.[38] Because only 2-fold averaging was possible with the S402P M_1-PK structure, the region around the site of mutation and regions of the B-domain which were not observed in the 1PKN structure, were in areas of weak electron density. These areas of the model were rebuilt using omit maps. Final refinement statistics are summarized in Table 2.

Protein Data Bank accession numbers

Coordinates of the rRMPK and the S402P structures have been deposited in the Protein Data Bank with entry numbers 1F3W and 1F3X, respectively.

Acknowledgements

Figure 3 was drawn with XTALVIEW.[39] All other figures were drawn with MOLSCRIPT.[40] All figures were rendered with RASTER3D.[41] A critical review of the manuscript by Drs Xiaodong Cheng and Werner Braun is appreciated. The research was supported by NIH grant GM-45579 and Robert A. Welch Foundation grants H-0013 and H-1238 to J.C.L., and H-1345 to R.O.F.

References

1. Ainsworth, S. & MacFarlane, N. (1973). A kinetic study of rabbit muscle pyruvate kinase. *Biochem. J.* **131**, 223-236.
2. Consler, T. G., Woodward, S. H. & Lee, J. C. (1989). Effects of primary sequence differences on the global structure and function of an enzyme: a study of pyruvate kinase isozymes. *Biochemistry,* **28**, 8756-8764.
3. Consler, T. G., Jennewein, M. J., Cai, G. Z. & Lee, J. C. (1992). Energetics of allosteric regulation in muscle pyruvate kinase. *Biochemistry,* **31**, 7870-7878.
4. Hall, E. R. & Cottam, G. L. (1978). Isozymes of pyruvate kinase in vertebrates: their physical, chemical, kinetic and immunological properties. *Int. J. Biochem.* **9**, 785-793.
5. Muirhead, H., Clayden, D. A., Barford, D., Lorimer, C. G., Fothergill-Gilmore, L. A., Schiltz, E. & Schmitt, W. (1986). The structure of cat muscle pyruvate kinase. *EMBO J.* **5**, 475-481.
6. Oberfelder, R. W., Barisas, B. G. & Lee, J. C. (1984). Thermodynamic linkages in rabbit muscle pyruvate kinase: analysis of experimental data by a two-state model. *Biochemistry,* **23**, 3822-3826.
7. Oberfelder, R. W., Lee, L.-Y. & Lee, J. C. (1984). Thermodynamic linkages in rabbit muscle pyruvate kinase: kinetic, equilibrium, and structural studies. *Biochemistry,* **23**, 3813-3821.
8. Consler, T. G. & Lee, J. C. (1988). Domain interaction in rabbit muscle pyruvate kinase. II. Small angle neutron scattering and computer simulation. *J. Biol. Chem.* **263**, 2787-2793.
9. Mattevi, A., Bolognesi, M. & Valentini, G. (1996). The allosteric regulation of pyruvate kinase. *FEBS Letters,* **389**, 15-19.
10. Friesen, R. H. E., Castellani, R. J., Lee, J. C. & Braun, W. (1998a). Allostery in rabbit pyruvate kinase: development of a strategy to elucidate the mechanism. *Biochemistry,* **37**, 15266-15276.
11. Cheng, X., Friesen, R. H. E. & Lee, J. C. (1996). Effects of conserved residues on the regulation of rabbit muscle pyruvate kinase. *J. Biol. Chem.* **271**, 6313-6321.
12. Friesen, R. H. E., Chin, A. J., Ledman, D. W. & Lee, J. C. (1998b). Interfacial communications in recombinant rabbit kidney pyruvate kinase. *Biochemistry,* **37**, 2949-2960.
13. Friesen, R. H. E. (1998). Effects of conserved residues on the allosteric regulation of pyruvate kinase: a structure-function study of rabbit muscle and kidney-pyruvate kinase. PhD thesis, Department of Human Biological Chemistry and Genetics, University of Texas Medical Branch at Galveston, TX.
14. Monod, J., Wyman, J. & Changeux, J.-P. (1965). On the nature of allosteric transitions: a plausible model. *J. Mol. Biol.* **12**, 88-118.
15. Heyduk, E., Heyduk, T. & Lee, J. C. (1992). Global conformational changes in allosteric proteins. A study of *Escherichia coli* cAMP receptor protein and muscle pyruvate kinase. *J. Biol. Chem.* **267**, 3200-3204.
16. Friesen, R. H. E. & Lee, J. C. (1998). The negative dominant effects of T340M mutation on mammalian pyruvate kinase. *J. Biol. Chem.* **273**, 14772-14779.
17. Larsen, T. M., Laughlin, L. T., Holden, H. M., Rayment, I. & Reed, G. H. (1994). Structure of rabbit muscle pyruvate kinase complexed with Mn^{2+}, K^{+}, and pyruvate. *Biochemistry,* **33**, 6301-6309.
18. Larsen, T. M., Benning, M. M., Wesenberg, G. E., Rayment, I. & Reed, G. H. (1997). Ligand-induced domain movement in pyruvate kinase: structure of the enzyme from rabbit muscle with Mg^{2+}, K^{+}, and L-phospholactate at 2.7 Å resolution. *Arch. Biochem. Biophys.* **345**, 199-206.
19. Larsen, T. M., Benning, M. M., Rayment, I., . & Reed, G. H. (1998). Structure of the bis(Mg^{2+})-ATP-oxalate complex of the rabbit muscle pyruvate kinase at 2.1 Å resolution: ATP binding over a barrel. *Biochemistry,* **37**, 6247-6255.
20. Jurica, M. S., Mesecar, A., Heath, P. J., Shi, W., Nowak, T. & Stoddard, B. L. (1998). The allosteric regulation of pyruvate kinase by fructose-1,6-bisphosphate. *Structure,* **6**, 195-210.
21. Gerstein, M. (1992). A resolution-sensitive procedure for comparing protein surfaces and its application to the comparison of antigen-combining sites. *Acta Crystallog. sect. A,* **48**, 271-276.
22. Rigden, D. J., Phillips, S. E. V., Michels, P. A. M. & Fothergill-Gilmore, L. A. (1999). The structure of pyruvate kinase from *Leishmania mexicana* reveals details of the allosteric transition and unusual effector specificity. *J. Mol. Bol.* **291**, 615-635.
23. Mattevi, A., Valentini, G., Rizzi, M., Speranza, M. L., Bolognesi, M. & Coda, A. (1995). Crystal structure of *Escherichia coli* pyruvate kinase type I: molecular basis of the allosteric transition. *Structure,* **3**, 729-741.
24. Burley, S. K. & Petsko, G. A. (1988). Weakly polar interactions in proteins. *Advan. Protein Chem.* **39**, 125-189.
25. Hunter, C. A. & Sanders, J. K. M. (1990). The nature of π-π interactions. *J. Am. Chem. Soc.* **112**, 5525-5534.
26. Hunter, C. A., Singh, J. & Thornton, J. M. (1991). π-π Interactions: the geometry and energetics of phenylalanine-phenylalanine interactions in proteins. *J. Mol. Biol.* **218**, 837-846.
27. Pan, H., Lee, J. C. & Hilser, V. J. (2000). Binding sites in *Escherichia coli* dihydrofolate reductase communicate by modulating the conformational ensemble. *Proc. Natl Acad. Sci. USA,* **97**, 12020-12025.
28. Ikeda, Y., Tanaka, T. & Noguchi, T. (1997). Conversion of non-allosteric pyruvate kinase isozyme into an allosteric enzyme by a single amino acid substitution. *J. Biol. Chem.* **272**, 20495-20501.
29. Ikeda, Y. & Noguchi, T. (1998). Allosteric regulation of pyruvate kinase M2 isozyme involves a cysteine residue in the intersubunit contact. *J. Biol. Chem.* **273**, 12227-12233.
30. Allen, S. C. & Muirhead, H. (1996). Refined three-dimensional structure of cat-muscle (M1) pyruvate kinase at a resolution of 2.6 Å. *Acta Crystallog. sect. D,* **52**, 499-504.
31. Jeong, H., Mason, S. P., Barabasi, A.-L. & Oltvai, Z. N. (2001). Lethality and centrality in protein networks. *Nature,* **411**, 41-42.
32. Otwinowski, Z. (1993). Denzo. In *Data Collection and Processing* (Sawyer, L., Isaacs, N. & Bailey, S., eds), pp. 56-62, SERC Daresbury Laboratory, Warrington, UK.
33. White, M. A., Watowich, S. J. & Fox, R. O. (1999). Calibration of spiral readout image plate detectors. *J. Appl. Crystallog.* **32**, 65-70.
34. Brünger, A. T. (1992). *X-PLOR Version 3.1. A System for X-ray Crystallography and NMR*, Yale University Press, New Haven, CT.
35. Brünger, A. T., Adams, P. D., Clore, G. M., Delano, W. L., Gros, P. & Grosse-Kunstleve, R. W. *et al.* (1998). Crystallography and NMR system: a new

software suite for macromolecular structure determination. *Acta Crystallog. sect. D,* **54**, 905-921.
36. Kleywegt, G. J. & Jones, T. A. (1994). Halloween … masks and bones. In *From First Map to Final Model* (Bailey, S., Hubbard, R. & Waller, D., eds), pp. 59-66, SERC Daresbury Laboratory, Warrington, UK.
37. Collaborative Computational Project Number 4 (1994). The CCP4 suite: programs for protein crystallography. *Acta Crystallog. sect. D,* **50**, 760-763.
38. Jones, T. A., Zou, J. Y., Cowan, S. W. & Kjelgaard, M. (1991). Improved methods for building protein models in electron density maps and the location of errors in theses models. *Acta Crystallog. sect. A,* **47**, 110-119.
39. McRee, D. E. (1999). XtalView/Xfit - a versatile program for manipulating atomic coordinates and electron density. *J. Struct. Biol.* **125**, 156-165.
40. Kraulis, P. J. (1991). MOLSCRIPT: a program to produce both detailed and schematic plots of protein structures. *J. Appl. Crystallog.* **24**, 946-950.
41. Merritt, E. A. & Bacon, D. J. (1997). Raster3D: photorealistic molecular graphics. *Methods Enzymol.* **277**, 505-524.

Edited by R. Huber

(Received 2 February 2001; received in revised form 23 July 2001; accepted 30 July 2001)